

Accepted Manuscript

Title: Pressure-assisted infiltration of molten metals into non-rigid, porous carbon fibre structures

Authors: H. Constantin, L. Harper, A.R. Kennedy

PII: S0924-0136(17)30579-4

DOI: <https://doi.org/10.1016/j.jmatprotec.2017.11.059>

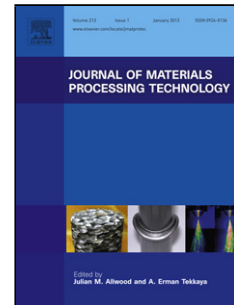
Reference: PROTEC 15533

To appear in: *Journal of Materials Processing Technology*

Received date: 12-9-2017

Revised date: 28-11-2017

Accepted date: 29-11-2017



Please cite this article as: Constantin, H., Harper, L., Kennedy, A.R., Pressure-assisted infiltration of molten metals into non-rigid, porous carbon fibre structures. *Journal of Materials Processing Technology* <https://doi.org/10.1016/j.jmatprotec.2017.11.059>

This is a PDF file of an unedited manuscript that has been accepted for publication. As a service to our customers we are providing this early version of the manuscript. The manuscript will undergo copyediting, typesetting, and review of the resulting proof before it is published in its final form. Please note that during the production process errors may be discovered which could affect the content, and all legal disclaimers that apply to the journal pertain.

<AT>Pressure-assisted infiltration of molten metals into non-rigid, porous carbon fibre structures

<AU>

<AU>H. Constantin^a, L Harper^a, A.R. Kennedy^{2b*}

##Email##a.kennedy3@lancaster.ac.uk##/Email## <AFF>^aFaculty of Engineering, University of Nottingham, Nottingham, NG7 2RD, UK.

<AFF>^b Department of Engineering, Lancaster University, Lancaster, LA1 4YW, UK.

<H1>3 <ABS-HEAD>Abstract

<ABS-P>Mercury intrusion porosimetry has been conducted on a range of non-rigid, porous carbon fibre structures. Comparison with data from gas pressure infiltration experiments in a molten Al-Si alloy shows it to be a useful tool in determining the pressure required to produce Al metal matrix composites with low levels of porosity. Whilst for non-rigid fibre preforms, as studied here, it is difficult to pin-point every aspect of the infiltration process, the method does give an indication of critical aspects of the infiltration behaviour. Preforms made from loose and spread tow can be fully infiltrated at relatively low pressures (12 bar) and although metal can fill the spaces between fibre bundles within textile-based preforms at low pressures, densely-packed bundles are only infiltrated at higher pressures, usually in excess of 50 bar. Mercury intrusion porosimetry could provide a valuable and simple tool in the design of fibre-reinforced metal matrix composites with optimised structures that are easy to manufacture.

<KWD>Keywords: Casting; infiltration; composites

<H1>1. Introduction

Infiltration processing is a versatile and cost effective method for the production of metal matrix composites (MMCs). By this procedure, molten metal is forced, using either mechanical or gas pressure, into the interstices or channels within a porous structure, commonly comprised of rigid packed beds of particles or fibres, with the aim being to fill all the available pore space and produce a dense product.

For polymer composites, where wetting between the resin matrix and fibre reinforcement is generally good, the key role of the applied pressure is to facilitate rapid transfer of high viscosity resin throughout the network of channels between and within the fibre bundles in the preform. Although Kennedy et al. (2000) showed, by example of spontaneous wetting of ceramic powders by molten Cu, that wetting can be good in some metal-ceramic systems and Gil and Kennedy (2012), that spontaneous wetting is also possible in Al-systems under certain tailored atmospheric conditions; generally, under normal processing conditions, wetting between Al alloys and most candidate ceramic reinforcements is poor. Kennedy and Karantzalis (1999) presented a large number of examples to confirm this, relating the non-wetting behaviour to contact angles that greatly exceed 90°. Despite low melt viscosities for molten metals, poor wetting necessitates the requirement for an external pressure to be applied for infiltration to take place. Being able to predict the pressure required to initiate the intrusion of liquid metal into a porous preform and the maximum pressure required to eliminate all the porosity, is paramount to designing preform structures and the apparatus required to affect infiltration.

5 <LIST ><4**1**>Mercury intrusion porosimetry (MIP) can be used to generate plots of the cumulative volume of liquid intruded into a rigid porous structure as a function of the pressure applied. These plots are characteristic of the pore size and geometry of the porous structure as well as intrinsic wetting characteristics for the system. These data can be readily converted into drainage curves; plots of the degree of filling (or saturation) of the porous structure, against pressure. Bahraini et al. (2005) used a bespoke high temperature porosimeter to demonstrate that drainage curves for a given porous structure, derived from

conventional Hg porosimetry (at room temperature) are of the same form as intrusion by molten metal at high temperature, since the infiltration paths are self-similar from one metal to the other, the only difference being the intrinsic wetting behaviour. Conversion from the Hg (MIP) to a molten Al system is then achieved by multiplying the Hg data by a scaling factor, ϕ , the ratio of the wetting behaviour (the magnitude of the work of immersion) in the Al-preform and Hg-preform systems. This factor is described by:

$$\phi = \frac{\cos(\theta_{Al-Pre}) \sigma_{LVAl}}{\cos(\theta_{Hg-Pre}) \sigma_{LVHg}} \quad (1)$$

where σ and θ are the surface tension and contact angle for the respective systems. This relationship has been shown to hold for rigid packed beds of particles of different morphologies, for materials including alumina and diamond (Bahraini et al., 2005), AlN (Kida et al., 2008), graphite (Molina et al., 2007) and SiC (Bahraini et al., 2008). Carbon fibres (CF) are ideal reinforcements for Al matrices as their high stiffness and low density offer the potential for achieving significant increases in the specific stiffness for the composite, over the base material. Carbon fibre composite fabrics are derived, in the main, from mm-sized bundles of carbon fibres (tow) which contain thousands of tightly-packed 5-10 μm diameter individual fibres. Research and development in carbon fibre polymer composites has seen the creation and implementation of diverse 2D and 3D fibre architectures to produce tailored mechanical properties, but the design of MMCs with CF reinforcement draws very little from the experiences in polymer systems, using mainly simple uni-directional and 3D random architectures.

This study applies MIP to a range of diverse CF architectures developed for wettable polymer resin systems, with the distinction from previous studies that these materials are not rigid structures nor do they possess simple pore geometries (unlike, for example, as achieved in packed powder beds). MIP observations are compared with data from Al-CF infiltration experiments at a range of pressures, with the aim being to establish whether this approach can be used to accurately predict the infiltration behaviour for molten Al within non-rigid structures containing multi-scale and complex pore structures and highlight any potential issues for using such products to produce Al-MMCs.

2. Experimental procedure

A selection of different CF preform architectures was used. These are listed in Table 1 and shown in Figure 1-4. A recycled carbon fibre (rCF) mat is shown in Figure 1, it is a non-woven, thin mat, made from off-cuts of SGL's 50K (a tow containing 50,000 fibres) non-crimp fabric. The chopped sections of fabric are "fluffed up" separating the fibre bundles, and then needle-punched to produce a widely-spaced mixture of randomly-orientated individual and loose discontinuous bundles of fibres, typically 60mm in length with an approximate volume fraction of 0.6.

Figure 2a shows a preform fabricated by crochet (Cro-CF). Crocheting is a process that uses a hook to fabricate a fabric from a continuous length of CF tow by creating loops. The crochet hook was 5 mm in diameter, which determined the size of the loops. Toray T700-60E 12K carbon fibre tow was crocheted into a flat strip with an approximate overall fibre fraction of 0.29, as is shown in Figure 2b.

A carbon fibre plain weave (WCF) was investigated, consisting of 6K carbon fibre bundles in the warp and weft directions, as shown schematically in Figure 3a, producing a mat with a fibre fraction of approximately 0.60. A 3D woven CF (3DWCF) preform was also studied, shown in Figure 4. The through-the-thickness weave had a binder-to-warp-stack ratio of 1:1, i.e. each binder tow was separated by one vertical stack of warp tows. This material contained an alternating stack of 9 weft layers and 8 warp layers, forming a dense 3D fabric that was approximately 3.5 mm thick. The carbon fibre tows were AKSACA A-38 with 6 K filaments

for the warp and weft tows, and 3 K filaments for binder tows. The fabric had an overall fibre volume fraction of approximately 0.55 and repeating units that are on a finer scale to that for the WCF material.

CF preforms were infiltrated using a gas pressure infiltration method (GPI), at a series of different pressures. Preforms were fabricated by die-cutting circular discs of diameter 28 mm from each of the CF fabrics, and stacking multiple discs within a 29 mm diameter alumina crucible (an example of stacked rCF fabric discs was shown in Fig 1c). The Cro-CF mat was rolled into a cylinder, as was shown in Figure 2c, before being loaded into the crucible. The Cro-CF, WCF and 3DWCF preforms weighed approximately 10g, but owing to the poor packing between the layers (loftiness) in the rCF preform, only 1.7g could be loaded into the crucible.

Approximately 60g of an Al–12 wt.% Si alloy was placed on top of the preforms and the assemblies were placed inside a bespoke pressure vessel. The vessel and its contents were heated to 550°C under vacuum for 1 h to remove sizing from the preforms, and then raised to 750°C and held for 1 h to allow the Al to melt and to form a liquid metal “seal” over the preform. Thereafter, Ar gas pressure was applied (at pressures ranging from 0.5 to 55 bar \pm 5%) for 30 min, followed by cooling and solidification under pressure. The GPI rig and a schematic of the internal setup are shown in Fig 5. MMCs were sectioned and mounted in conductive resin, polished to a 1 μ m diamond finish and studied using an optical microscope. MIP data were obtained using a Micrometrics Autopore 4 Hg Porosimeter, at mercury pressures from 0.06 to 100 bar, using the largest available penetrometer size (25 mm in diameter and length). Samples were prepared in the same way for the penetrometer as for infiltration with Al, but using a 22 mm diameter cutter.

3. Results and Discussion

Data before the onset and at the end of MIP measurements yield values for the bulk and apparent densities of the preforms. The bulk density indicates the amount of uninfiltrated space within the preform, influenced by the separation between the layers in the multi-layered structure and any compression of this structure caused by the pre-stress from the Hg in the penetrometer (approximately 0.006 MPa). The apparent density, taken at the end of the pressurisation cycle, should, if all the porosity is interconnected and the preform is fully infiltrated, be equal to the density of the carbon fibres.

Despite the relatively high fraction of fibres in the rCF mat, the preform fibre fraction, calculated from the bulk density, was only 0.12, demonstrating the high degree of separation between the layers (loft) prior to infiltration. The fibre fraction estimated from the bulk density in the Cro-CF sample was 0.52, indicating either some compression of the preform when first filling with Hg or, more likely, permeation of Hg into the void spaces within the preform, via the large pores (loops) that are unique to this structure. The bulk densities for the WCF and 3DWCF samples were 0.50 and 0.62 respectively (compared with 0.60 for the WCF mat and 0.55 for the 3DWCF), suggesting some separation between the layers in the multi-layered WCF preform and a small degree of compression of the 3DWCF preform at the minimum Hg pressure. In all cases, the apparent density for the preforms, taken at the maximum intrusion pressure (100 bar) was greater than 99% of the estimated fibre density, indicating, within experimental error, that complete infiltration (saturation) had taken place. Figure 6 shows the MIP data for intrusion with Hg, normalised with respect to the maximum volume intruded, giving the fraction of saturation as a function of pressure. Each of the plots exhibits a linear region at lower pressures, which is a result of compression of the preforms before infiltration takes place. These regions are more evident for the more compliant structures (those with steeper gradients of saturation vs. pressure) such as the rCF and WCF preforms, which show similar behaviour, compressing readily as the spaces between the thin, lofty, multi-layered laminates are removed. The 3DWCF sample, made from denser, thicker

discs and the crocheted sample, in which the large void spaces within the links are already filled with Hg before pressure is applied, behave in a similar way and are more than 10 times stiffer than the other preforms.

The linear preform compression regions could be removed from the MIP plots, making the saturations a more accurate representation of the degree of filling with Hg but, since it is the points at which there are steps in the saturation and where the saturation reaches unity that are of primary importance, for simplicity, this adjustment has not been made.

None of the plots are continuous curves, with steps and plateaus (marked on these traces with vertical dotted lines) that are characteristic of multi-scale porosity within the complex architectures. Steps in the curves mark rapid increases in the degree of filling with an increment in pressure and are often characteristic of the pressure attaining a critical level such that mercury can now flow through small constrictions to reach large open volumes. Plateaus indicate an arrest in the filling behaviour, despite significant increases in pressure, typical of an absence of pores in the structure spanning a specific size range. The relatively simple rCF preform structure shows a transition in the infiltration process at 0.3 bar, high saturation above 0.6 bar and complete saturation above 5 bar. The other three preforms show different initial filling characteristics but share an arrest in this behaviour, followed by a plateau, beginning at 1.4 bar. Filling of the preform resumes at slightly different pressures for these 3 preforms, with clear arrests at 6.0 and 12.0 bar for the WCF and 3DWCF preforms respectively. At high pressures the interdependence between pressure and saturation shows multiple undulations, reflecting a highly complex preform structure, in particular, as expected, for the 3DWCF material. The pressures for complete saturation of the textile-based preforms are more than 5 times higher than that for the rCF preform with that for the 3DWCF preform being more than 7 times higher.

The key transitions in the infiltration behaviour can be related to structural facets in the preform via the Young-Laplace equation, which relates the applied pressure, P , to the minimum pore diameter, d , through which metal can flow.

$$d = \frac{4\sigma_{Hg}\cos\theta}{P} \quad (2)$$

Although there are no data for the contact angle for Hg on CF, there are data for wetting of graphite, but they are highly variable. Molina et al. (2007) reported values ranging between 112° and 142° , with 140° being commonly accepted, but justifying their own choice of 124° for use in further analysis of their data. Figure 7 plots the MIP data in Figure 6, converting the applied pressure to an equivalent pore diameter using equation 1 with a Hg surface tension of 486 mJ m^{-2} and a contact angle of 124° . Transitions at similar pore sizes, for different preform materials, indicate they share similar structural features, no doubt originating from the fibre bundles from which they are derived. Table 2 gives the key transition pressures and capillary diameters, presented as a range using contact angles of both 124° and 140° . It is clear that capillaries on the scale of roughly $10\mu\text{m}$ present an early barrier to infiltration for textile materials and that complete filling requires penetration of capillaries that are sub-micron in size.

Table 2 also presents the equivalent pressure at which the same transitions would be expected in the high temperature Al-Si alloy system. In the absence of data for the CF system, data from Molina et al. (2007) for Al-Si on graphite ($\phi = 2.4$) has been used. It is anticipated that this multiplier provides a cautious estimate of the pressure that will be needed for Al infiltration, since it uses the contact angle data at the upper range of those typically reported for Al and at the lower range of those reported for Hg.

The estimated pressures were used to inform the choice of experimental infiltration trials and Figure 8 shows a revised version of Figure 6, adapted to predict the infiltration behaviour in

the Al-Si system, with pressures at which infiltration trials were conducted marked on the relevant traces and labelled corresponding to micrographs in Figures 9 to 12.

Figure 9 shows optical micrographs for rCF/Al-12Si MMCs fabricated at 0.5, 1 and 12 bar gas pressure. In all cases, dispersed, individual fibres can be seen, as can small bundles that are residual tow that was not broken-up during the manufacturing process. Numerous macrovoids are evident for infiltration at 0.5 bar, and the inset image in Figure 9a shows a typical fibre bundle, which has not been infiltrated. At 1 bar gas pressure, no macro voids were observed, only at a higher magnification could micro voids within fibre bundles be observed (see inset image in Figure 9b). At 12 bar gas pressure the voids within the fibre bundles were eliminated and the fibre preform was deemed to be fully infiltrated. These observations agree well with the predicted behaviour from the saturation-pressure plot in Figure 8. Low pressures (<0.5 bar) enable metal to infiltrate the large spaces between the dispersed individual fibres and bundles and although the saturation increases with increasing pressure, this pressure is not sufficient to enable metal to penetrate the fibre bundles. At 12 bar pressure the corresponding capillary diameter is less than 3 μm and Figure 9c shows that is sufficient to allow infiltration into the splayed, unconstrained fibre bundles that are present in this preform, resulting in extremely low levels of porosity.

Figure 10 shows images for WCF/Al-12Si MMCs fabricated using 5, 15 and 55 bar infiltration pressures. At 5 bar infiltration pressure, although the regions between the bundles have been filled with Al, the majority of the fibre bundles have not been infiltrated, but there are some areas at the perimeter of the bundles that are beginning to be infiltrated and this may be due spreading of the fibre bundles at the unconstrained, "free" edges of the preform, where it was stamped. At 15 bar infiltration pressure, as predicted by the saturation curves, there is a step change in infiltration and many of the fibre bundles have been partially infiltrated. At 55 bar, infiltration is near fully complete, with only some low level intra-bundle porosity observable at the centre of the bundles (which it is possible could have been removed with a longer infiltration time). The corresponding capillary diameter at this pressure is 0.5-0.7 μm , similar in scale to that for the gaps between fibres in these tightly-bound bundles (in which the fibres are more densely-packed and are more firmly constrained than is the case for the rCF).

Figure 11 shows microstructures for Cro-CF/Al-12Si MMCs fabricated using 5, 25 and 50 bar infiltration pressures. At the lowest pressure, metal fills the inter-bundle regions, but black regions of fibre bundles that have not been infiltrated are visible. When the pressure is increased to 25 bar (Figure 11b), outer regions of the bundles, that have been partly spread during the crochet process, have been infiltrated (grey areas), whilst the more densely-packed fibres at the centres of the bundles have not yet been filled. Figure 8 indicates that the saturation at this pressure is reasonably low (0.6) and significantly lower than for the WCF preform (0.82). The micrographs in Figures 10 and 11 do not support either the low levels of saturation or the large difference between the 2 preform types. This highlights how caution must be exercised when comparing absolute values for the saturation if compensation has not been made for either pre-compression or pre-infiltration of the preform before the MIP data are recorded. Figure 11c shows that at 50 bar the fibre bundles appear well infiltrated with the exception of a few small areas of porosity within the bundles, as indicated in Figure 11c by a white circle. Again the behaviour observed is a good fit to the saturation – pressure curve, where the predicted pressure for complete saturation for Al is 54 bar, similar to that for the WCF preform, indicating that, as expected, affecting infiltration within the spaces between fibres in the tightly-bound tow enables complete infiltration to be attained.

3DWCF/Al-12Si MMCs were fabricated using 5, 15 and 55 bar infiltration pressures. At 5 bar pressure, no infiltration of the 3DWCF preform occurred, suggesting that the early stages of this curve are dominated by compression, rather than infiltration, of this dense 3D preform

which is of a finer scale than the WCF textile. Some infiltration was observed at the equivalent (lower) pressure for Hg and this highlights that for non-rigid preforms, such as those investigated in this work, the magnitude of the onset pressure for infiltration will more greatly affect the extent of prior elastic or plastic deformation of the preform and the concomitant reduction in fibre or tow spacing, thereby raising the pressure necessary for infiltration. This effect will reduce the accuracy of the translation of MIP data to molten metal systems. Figure 12a shows a 3DWCF/Al-12Si MMC fabricated using 15 bar infiltration pressure, where the spaces between the fibre bundles have been infiltrated, but the bundles have only been partially filled (as per the other fabric structures). At 55 bar many of the fibre bundles are filled, as was the case for previous observations, but there are still large areas of porosity, shown in Figure 12b. The saturation curve indicates that pressures in excess of 80 bar are needed for complete infiltration of this complex architecture and, since the fibre spacings within the rigid bundles are not likely to differ much from the other fabrics based on woven tow structures, it is probable that within this dense 3D woven preform structure there are "bottleneck" constrictions at fibre bundle contact points, that are of the order of 0.3-0.4 μm in diameter, that prevent metal flow to some regions of the preform. These constrictions are likely to form, or close, when increasing pressure is applied to the preform before the onset of the intrusion process.

The methodology presented, despite some concerns as to the accuracy of the transposition of some of the wetting data to the CF systems, has been shown to be a reliable predictor of not only the maximum pressure required to affect complete infiltration of a number of different non-rigid, porous CF preform structures, but also is a reliable indicator of critical pressures required to affect step changes in the infiltration process. For example, the plateaus observed in Figure 6 at pressures close to 1 bar, mark the complete filling of the large spaces between the fibre bundles (inter-bundle intrusion) at low pressure, with a cessation of intrusion, until a recommencement at higher pressures, corresponding to filling of the much smaller gaps between fibres in the bundles (intra-bundle intrusion). This enables fruitful comparisons for the infiltration behaviour of similar materials with different architectures.

There are, however, clearly some shortcomings in the interpretation of the MIP data for these complex, non-rigid preform structures, owing to the possibilities of pre-infiltration of very large pores before the MIP process commences and pre-compression of either multi-layered preforms with high loft, or preforms with small pores, before the onset of infiltration. Since these complex preforms may exhibit all these characteristics, it is very difficult to isolate each contribution and make accurate corrections to the MIP plots. This makes investigations of this kind more complex than that by, for example, Gil et al. (2012) that used rigid packed beds or rigid porous structures, from which the degree of saturation was readily calculated and accurately corrected. This then limits the utility of the saturation-pressure plots for compressible preforms, most notably, accurate determination of the level of porosity as a function of infiltration pressure below the maximum is difficult to determine from MIP data. A comparison with real porosity levels in the resulting MMCs, measured from the density or by quantitative microscopy, is also difficult owing to compression and relaxation of the non-rigid preforms, in which the final fibre fraction is therefore uncertain, in addition to trying to account for porosity which may form due to solidification shrinkage.

That said, the findings and methodologies arising from this study could well be a potent tool to assess the suitability of a wide variety of existing CF architectures, which have been designed for polymer-based systems where wetting isn't the problem, and determine how they might be re-engineered or modified to be more suitable for infiltration by molten metals. The key issue that can be addressed in this way is avoiding excessive compression of the preform, which induces variability in preform density, has the potential to reduce the size or even block off passages to liquid in the preform and can cause fibre damage. MIP could be

used to assess the viability of solutions that avoid the over-use of undesirable preform binding agents but involve creating multi-scale porosity within the fibre architectures to stagger the ingress of molten metal and increasing inter-fibre spacings within the fibre bundles (and thereby reducing the maximum infiltration pressure) by spreading the tow, pre- or post- preform manufacture.

It is worthy of note that reactions between the fibres and the matrix, to form micron-scale blocky Al_4C_3 particles that are commonly reported for this system, were not noticeable (exemplified most clearly in Figure 11c). Grinding and polishing with water was avoided in order to eliminate the potential for removal of the hygroscopic carbide and thus the absence of reaction layers or pitting around the fibres is testimony to the absence of noticeable reaction, most likely aided by the relatively short exposure times between the fibres and molten metal.

5. Conclusions

MIP is a useful method for comparing metal infiltration into different preform types; it allows insight into the structure of preforms and crucially, the pressure required for full saturation (or acceptable levels of residual porosity). It is difficult to pin-point every aspect of the infiltration process by MIP alone, owing to the compressibility of the preforms used in this study, but the procedure gives an indication of critical aspects of the infiltration behaviour. It has confirmed preforms made from loose and spread tow can be fully infiltrated at relatively low pressures (12 bar) and that although metal can fill the spaces between fibre bundles within textile-based preforms at low pressures, densely-packed bundles are only infiltrated at higher pressures, usually in excess of 50 bar. The process and alloy system give rise to composites that were free from reaction products at the fibre-matrix interface.

References

<BIBL>

- Bahraini, M., Molina, J.M., Kida, M., Weber, L., Narciso, J., Mortensen, A.,;1; 2005. Measuring and tailoring capillary forces during liquid metal infiltration. *Current Opinion in Solid State and Materials Science*, **9** (4–5) 196-201.
- Bahraini, M., Molina, J.M., Weber, L., Mortensen, A.,;1; 2008. Direct measurement of drainage curves in infiltration of SiC particle preforms, *Mater Sci and Eng A*, **495**, 203-207
- Gil, R., Jinnapat, A., Kennedy, A.R.,;1; 2012, Pressure-assisted infiltration of molten aluminium into open cell ceramic foams: Experimental observations and infiltration modelling. *Composites Part A: Applied Science and Manufacturing*, **43**, 880 - 884.
- Gil, R., Kennedy, A.R.,;1; 2012. Capillarity-driven infiltration of alumina foams with an Al-Mg alloy: Processing, microstructure, and properties, *Journal of Materials Engineering and Performance*, **21**, 5, 714-720.
- Kennedy, A.R., Karantzalis, A.E.,;1; 1999. The Incorporation of Ceramic Particles into Molten Al and the Relationship to Contact Angle Data, *Mater. Sci. and Eng. A264*, 122-129.
- Kennedy, A.R., Wood, J.D., Weager, B. M.,;1; 2000. The Wetting and Spontaneous Infiltration of Ceramics by Molten Copper, *J Mat Sci*, **35**, 2909-2912.
- Kida, M., Bahraini, M., Molina, J.M., Weber, L., Mortensen A.,;1; 2008. High-temperature wettability of aluminum nitride during liquid metal infiltration, *Mater Sci and Eng A*, **495**, 197-202.
- Molina, J.M., Rodriguez-Guerrero, A., Bahraini, M., Weber, L., Narciso, J., Rodriguez-Reinoso, F., Louis, E., Mortensen, A.,;1; 2007. Infiltration of graphite preforms with Al–Si eutectic alloy and mercury, *Scripta Mater*, **56**, 991–994.

</BIBL>

<Figure>Figure 1. rCF mat, (a) showing the overall structure, (b) showing individual fibres, split tow and some sparse areas with few fibres and (c) an rCF preform made from stacked discs

<Figure>Figure 2. Crocheted CF (Cro-CF) showing (a) a simple chain, (b) a flat crocheted CF strip, and (c) a strip rolled into a cylinder to make a preform.

<Figure>Figure 3. Woven CF mat (WCF) showing (a) a schematic illustration of the fibre architecture and (b) the fabric.

<Figure>Figure 4. 3D Woven CF mat (3DWCF) showing (a) a schematic illustration of the fibre architecture and (b) the fabric in plan view.

<Figure>Figure 5. Photo of the GPI rig (a) and (b) schematic cross section showing, (i) pressure gauge, (ii) argon gas bottle, (iii) thermocouple, (iv) crucible containing Al and CF.

<Figure>Figure 6. MIP data for the four preform types, showing pressure against preform saturation; significant transitions have been marked on these traces with vertical dotted lines

<Figure>Figure 7. Pore diameter plotted against saturation from MIP data, with data for lower diameters inset.

<Figure>Figure 8. Revised intrusion plots for Al, using a multiplier of 2.4. Labels correspond to images for MMCs fabricated at different pressures in Figures 9-12.

<Figure>Figure 9. Optical microscope images of rCF/Al-12Si MMC fabricated using a) 0.5, b) 1 and c) 12 bar gas pressure.

<Figure>Figure 10. Optical microscope images of WCF/Al-12Si fabricated using (a) 5 bar, (b) 15 bar, (c) 55 bar gas pressure, inset image shows intra-bundle infiltration and porosity

<Figure>Figure 11. Optical microscope images of Cro-CF/Al–12Si fabricated using (a) 5 bar, (b) 25 bar, (c) 50 bar gas pressure, inset image shows intra-bundle infiltration, intra-bundle porosity is highlighted with a white circle

<Figure>Figure 12. OM images of 3DWCF/Al–12Si fabricated using (a) 15 bar, (b) 55 bar gas pressure, inset image shows intra-bundle porosity.

<Table>Table 1. CF preform types used to fabricate MMCs

Preform	Fibre type	Construction	Tow size
rCF	Recycled (60mm fibre length)	Non-woven	N/A
Cro-CF	T700SC	Crocheted	12K
WCF	HTS40	Plain weave	6K
3DWCF	ASKACA A-38	3D weave	6K warp/weft 3K binder

<Table>Table 2. Preform types and associated pressures (P, in bar) and capillary diameters (d, in μm) for critical steps in the MIP process, showing the range in values of capillary diameter for contact angles between 124° and 140° .

	End of 1 st curve			End of plateau			Full saturation		
	P _{Hg}	P _{Al}	d	P _{Hg}	P _{Al}	d	P _{Hg}	P _{Al}	d
rCF	0.3	0.7	36.2-49.6	-	-	-	5.0	12.0	2.2-3.0
Cro-CF	1.4	3.4	7.8-10.6	1.5	3.6	7.2-9.9	22.7	54.5	0.5-0.7
WCF	1.4	3.4	7.8-10.6	2.5	6.0	4.3-6.0	22.6	54.2	0.5-0.7
3DWCF	1.4	3.4	7.8-10.6	2.6	6.2	4.2-5.7	35.6	85.4	0.3-0.4

<Figure>Figure and Table Captions

<Table>Table 3. CF preform types used to fabricate MMCs

<Table>Table 4. Preform types and associated pressures (P, in bar) and capillary diameters (d, in μm) for critical steps in the MIP process, showing the range in values of capillary diameter for contact angles between 124° and 140° .

<Figure>Figure 3. rCF mat, (a) showing the overall structure, (b) showing individual fibres, split tow and some sparse areas with few fibres and (c) an rCF preform made from stacked discs

<Figure>Figure 4. Crocheted CF (Cro-CF) showing (a) a simple chain, (b) a flat crocheted CF strip, and (c) a strip rolled into a cylinder to make a preform.

<Figure>Figure 3. Woven CF mat (WCF) showing (a) a schematic illustration of the fibre architecture and (b) the fabric.

<Figure>Figure 4. 3D Woven CF mat (3DWCF) showing (a) a schematic illustration of the fibre architecture and (b) the fabric in plan view.

<Figure>Figure 5. Photo of the GPI rig (a) and (b) schematic cross section showing, (i) pressure gauge, (ii) argon gas bottle, (iii) thermocouple, (iv) crucible containing Al and CF.

<Figure>Figure 6. MIP data for the four preform types, showing pressure against preform saturation; significant transitions have been marked on these traces with vertical dotted lines

<Figure>Figure 7. Pore diameter plotted against saturation from MIP data, with data for lower diameters inset.

<Figure>Figure 8. Revised intrusion plots for Al, using a multiplier of 2.4. Labels correspond to images for MMCs fabricated at different pressures in Figures 9-12.

<Figure>Figure 9. Optical microscope images of rCF/Al-12Si MMC fabricated using a) 0.5, b) 1 and c) 12 bar gas pressure.

<Figure>Figure 10. Optical microscope images of WCF/Al-12Si fabricated using (a) 5 bar, (b) 15 bar, (c) 55 bar gas pressure, inset image shows intra-bundle infiltration and porosity

<Figure>Figure 11. Optical microscope images of Cro-CF/Al-12Si fabricated using (a) 5 bar, (b) 25 bar, (c) 50 bar gas pressure, inset image shows intra-bundle infiltration, intra-bundle porosity is highlighted with a white circle

<Figure>Figure 12. OM images of 3DWCF/Al-12Si fabricated using (a) 15 bar, (b) 55 bar gas pressure, inset image shows intra-bundle porosity.

TDENDOFDOCTD

ACCEPTED MANUSCRIPT